JOURNAL OF THERMOPHYSICS AND HEAT TRANSFER
Vol. 17, No. 1, January–March 2003

Solutal Convection During Growth of Alloyed Semiconductor Crystals in a Magnetic Field

Nancy Ma*
North Carolina State University, Raleigh, North Carolina 27695

This paper presents a model for the unsteady species transport during bulk growth of alloyed semiconductor crystals with a planar crystal-melt interface and with an externally applied steady axial magnetic field. During growth of alloyed semiconductors such as germanium-silicon (GeSi) and mercury-cadmium-telluride (HgCdTe), the solute's concentration is not small so that density differences in the melt are very large. These compositional variations drive compositionally driven buoyant convection, or solutal convection, in addition to thermally driven buoyant convection. These buoyant convections drive convective transport, which produces nonuniformities in the concentration in both the melt and the crystal. This transient model predicts the distribution of species in the entire crystal.

Introduction

BECAUSE molten semiconductors are excellent electrical conductors, the melt motion and species transport can be controlled by an externally applied steady magnetic field during the growth process. The infinite number of possible magnetic field configurations provides the ability to tailor the melt motion in order to optimize the properties of the crystal. It is crucial that the distributions of species are as uniform as possible. When only a few devices were produced on surfaces of thin wafers sliced from a crystal, large compositional deviations could be tolerated because the devices were large enough to see the local average. With recent manufacturing advances millions of devices are now produced on a single wafer, so that even a small local compositional variation can lead to the malfunction of a single device.

During crystal growth without a magnetic field, oscillatory melt motions produce undesirable spatial oscillations of the concentration in the crystal. An externally applied magnetic field can be used to create a body force that provides an electromagnetic (EM) damping of the melt motion and to eliminate oscillations in the melt motion and thus in the composition of the crystal. Chedzey and Hurle[1] and Utech and Flemings[2] published the first papers to demonstrate the benefits of applying magnetic fields during semiconductor crystal growth. Unfortunately, the elimination of mixing and a moderate EM damping of the residual melt motion can lead to a large variation of the crystal's composition in the direction perpendicular to the growth direction (lateral or radial macrosegregation).[3]

If the EM damping is extremely strong, then the melt motion is suppressed and has no effect on the composition in the crystal, and this diffusion-controlled species transport might produce a radially and axially uniform composition in the crystal.[3] To achieve diffusion-controlled species transport, the species transport Péclet number $Pe_m = U_c L/D$ must be small, where U_c is the characteristic velocity for the magnetically damped melt motion and is inversely proportional to the square of the magnetic flux density B, while L is the characteristic dimension of the melt and D is the diffusion coefficient for the species in the molten semiconductor. If $Pe_m \ll 1$, then the characteristic ratio of convection to diffusion of the species is small, and the species transport is diffusion controlled. However, because typical values of D are 1 to 2×10^{-8} m^2/s, B must be extremely large for diffusion-controlled species transport on Earth. It is more practical to use magnetic fields that are strong enough to eliminate flow oscillations but that only moderately damp the residual steady melt motion, that is, for which Pe_m is still large and convection of species is important. With such fields the objective is to tailor the transport in order to achieve both lateral and axial compositional uniformity in the crystal. At each stage during the growth of a crystal by any process, there are infinitely different ways to tailor the strength and configuration of the externally applied magnetic field, the distribution of heat flux into the melt, etc., so that process optimization through trial-and-error experimental crystal growth is not practical. Models that accurately predict the composition in the entire crystal for any combination of process parameters are needed to facilitate process optimization.

During Bridgman growth of alloyed semiconductors, the application of magnetic fields have shown great promise. For example, Watring and Lehoczky[4] have shown that the radial variation between the maximum and minimum concentrations can be decreased by more than a factor of three with the application of a 5 T magnetic field. In these experiments one compositional profile indicated only a 0.04 mole fraction difference of CdTe in the radial macrosegregation of a mercury-cadmium-telluride (HgCdTe) crystal,[4] arising because the magnetic field retards the sinking of the heavier melt to the center of the ampoule resulting in less radial segregation. Ramachandran and Watring[5] reported a reduction in the radial segregation in all of their samples, which were grown in a magnetic field. Watring[6] found that radial uniformity sometimes occurred with weaker fields.

For alloyed semiconductors the density differences caused by compositional variations in the melt are very large. The rejected component, for example, Ge in GeSi or HgTe in HgCdTe, is generally much heavier than the other component, so that the melt's density is dramatically increased near the crystal-melt interface. In germanium-silicon (GeSi), for example, the mole fraction of germanium can vary from 0.95 in the melt, which has not yet received any rejected germanium to 0.99 near the interface, and this compositional difference corresponds to a density difference of nearly 300 kg/m^3. In a frequently used extension of the Boussinesq approximation, the melt density is assumed to vary linearly with both the temperature and mole fraction of either species. In this approximation the magnitudes of the density difference and of the resultant buoyant convection associated with the temperature variation or with the compositional variation can be characterized by $\beta_T(\Delta T)_0$ or $\beta_C(\Delta C)_0$, respectively, where β_T and β_C are the thermal and compositional coefficients of volumetric expansion and $(\Delta T)_0$ and $(\Delta C)_0$ are the characteristic radial temperature difference and the characteristic radial difference in the mole fraction of one species,

Received 7 February 2002; revision received 17 June 2002; accepted for publication 10 September 2002.

*Assistant Professor, Department of Mechanical and Aerospace Engineering, Campus Box 7910; nancy_ma@ncsu.edu. Member AIAA.

for example, of the mole fraction of silicon in the GeSi melt. For GeSi with $(\Delta T)_0 = 10$ K and $(\Delta C)_0 = 0.04$, the characteristic ratio of the buoyant convection driven by thermal variations to that driven by compositional variations is $\beta_T(\Delta T)_0/\beta_C(\Delta C)_0 = 0.1$. For a typical Bridgman process for HgCdTe, this ratio is approximately 0.01. Although the thermally driven buoyant convection is probably not negligible, particularly far from the crystal-melt interface where compositional variations are small, the compositionally driven buoyant convection or solutal convection is dominant particularly near the interface.

In the 1970s Hart[7] presented an asymptotic and numerical solution for the motion of a stratified salt solution in a two-dimensional container with both thermally driven and compositionally driven convection and without a magnetic field. In two recent studies[8,9] we investigated the effect of buoyant convections with a magnetic field and with solidification. Hirtz and Ma[8] investigated the effect of thermally driven buoyant convection on the dilute transport of silicon in a germanium melt, while Ma[9] investigated the effect of compositionally driven buoyant convection on the solutal transport in a nondilute mixture of silicon and germanium. In the present paper extend this classical problem[7] to include solidification in a steady axial magnetic field for the first time. We use a two-dimensional model problem in a horizontal container in order to provide physical insight and illustrate an asymptotic method, but the extension to three-dimensional melt motions in actual crystal-growth processes would be straightforward.

Hurle and Series[10] reviewed the pre-1994 literature on the use of magnetic fields during semiconductor crystal growth, with an emphasis on segregation during melt growth. Recently, Garandet and Alboussière[11] reviewed the literature on modeling and experimental studies of Bridgman growth in a magnetic field, while Walker[12] reviewed the use of asymptotic methods in the modeling of melt motion, heat transfer, and species transport during crystal growth with magnetic fields. Walker and Ma[13] reviewed convective species transport during crystal growth with steady magnetic fields. Our Pe_m is the same as the parameter ScGr/Ha[2] used by some other researchers,[14] where *Sc*, *Gr*, and *Ha* are the Schmidt, Grashoff, and Hartmann numbers, respectively.

Problem Formulation

We treat the unsteady, two-dimensional species transport of a species in a solidifying, electrically conducting semiconductor melt in a horizontal, rectangular container with thermally insulated top and bottom walls and with an externally applied, uniform, horizontal (axial) magnetic field $B\hat{\boldsymbol{x}}$. Here, B is the magnetic flux density, and $\hat{\boldsymbol{x}}$, $\hat{\boldsymbol{y}}$, and $\hat{\boldsymbol{z}}$ are the unit vectors for the Cartesian coordinate system. Our dimensionless problem is sketched in Fig. 1. The coordinates and lengths are normalized by half the distance between the top and bottom walls L, and a is the dimensionless length of the container.

Experiments[4] have shown that magnetic fields can control compositionally driven buoyant convection so that the electromagnetic body force must be comparable to the characteristic gravitational body force associated with compositional variations. Because the electric currents only arise from melt motions across the magnetic field, the magnetic field can damp the motion but cannot completely suppress it. Therefore, this balance gives a characteristic velocity for the magnetically damped compositionally driven buoyant convection[9]

$$U_c = \frac{\rho_0 g \beta_c C_0}{\sigma B^2} \tag{1}$$

where ρ_0 is the melt's density at the solidification temperature T_0, $g = 9.81$ m/s^2, and σ is the electrical conductivity of the melt. Thus we can expect the melt motion to decrease roughly as B^{-2} as the magnetic field strength is increased. For the growth of germanium-silicon crystals with $C_0 = 0.04$, the characteristic value varies from $U_c = 0.1348$ m/s for $B = 0.1$ T to $U_c = 5.3937 \times 10^{-5}$ m/s for $B = 5$ T.

The electric current in the melt produces an induced magnetic field that is superimposed on the applied magnetic field produced by the external magnet. The characteristic ratio of the induced to the applied magnetic field strengths is the magnetic Reynolds number

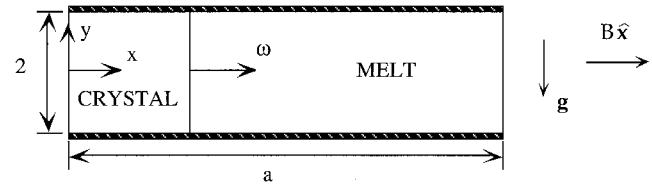

Fig. 1 Two-dimensional model problem with a uniform, steady, axial magnetic field $B\hat{\boldsymbol{x}}$ and with coordinates normalized by half the distance between the top and bottom walls.

$$R_m = \mu_p \sigma U_c L \tag{2}$$

where μ_p is the magnetic permeability of the melt. For all crystal-growth processes $R_m \ll 1$, and the additional magnetic fields produced by the electric currents in the melt are negligible.

In our two-dimensional model problem nothing varies in the z direction, and there can be a uniform electric field in the z direction E_z. In any actual horizontal Bridgman process there are electrically insulating walls at, say, $z = \pm d$, which block any electric current in the z direction. For the present recirculating flow $E_z = 0$ for zero net electric current. Ohm's law gives $\boldsymbol{j} = -v\hat{\boldsymbol{z}}$ for the electric current density normalized by $\sigma U_c B$, where $\boldsymbol{v} = u\hat{\boldsymbol{x}} + v\hat{\boldsymbol{y}}$ is the dimensionless melt velocity. Here, u and v are the horizontal and vertical velocities, respectively, normalized by U_c.

We assume that the temperature differences and compositional variations are sufficiently small so that all of the physical properties of the melt can be considered uniform and constant except for the density in the gravitational body force term of the momentum equation. In this Boussinesq-like approximation the characteristic temperature difference $(\Delta T)_0$ and characteristic mole fraction variation $(\Delta C)_0$ are assumed to be sufficiently small so that the melt's density is a linear function of temperature and composition, given by

$$\rho = \rho_0\left[1 - \beta_T\left(T^* - T_0\right) - \beta_c\left(C^* - C_0\right)\right] \tag{3}$$

and that $\beta_T(\Delta T)_0 \ll 1$ and $\beta_c(\Delta C)_0 \ll 1$, where T^* is the temperature in the melt, C^* is the mole fraction of one species in the melt, and C_0 is the initially uniform mole fraction in the melt before crystal growth begins.

In the Navier–Stokes equation the characteristic ratio of the EM body force term to the inertial terms is the interaction parameter $N = \sigma^2 B^4 L/\rho_0^2 g \beta_c C_0$. In a recent study[15] we investigated the role of inertia on the thermally driven buoyant convection during liquid-encapsulated growth of compound semiconductors and determined the errors associated with the neglect of inertial effects for interaction parameters between $N = 1.307$ and 6803.5. We found that inertia significantly affects the buoyant convection for which $N = 1.037$. As the interaction parameter is increased from this value, the ratios of the inertial force to the EM body force decrease. We found that the error caused by neglect of inertial effects is only 2.7% for $N = 16.59$ and is totally negligible for $N \geq 648.1$.

The equations governing the inertialess melt motion, heat transfer, and species transport are

$$-\nabla p + (\gamma T + C - 1)\hat{\boldsymbol{y}} - v\hat{\boldsymbol{y}} + Ha^{-2}\nabla^2 \boldsymbol{v} = 0 \tag{4a}$$

$$\nabla \cdot \boldsymbol{v} = 0 \tag{4b}$$

$$Pe_t\left[\frac{\partial T}{\partial t} + (\boldsymbol{v} \cdot \nabla)T)\right] = \nabla^2 T \tag{4c}$$

$$Pe_m\left[\frac{\partial C}{\partial t} + (\boldsymbol{v} \cdot \nabla)C)\right] = \nabla^2 C \tag{4d}$$

$$C = \frac{C^*}{C_0} \tag{4e}$$

$$T = \frac{T^* - T_0}{(\Delta T)_0} \tag{4f}$$

$$\gamma = \frac{\beta_T(\Delta T)_0}{\beta_c C_0} \tag{4g}$$

where T is the deviation of the dimensional melt temperature from the solidification temperature normalized by $(\Delta T)_0$ and $C(\xi, y, t)$ is the mole fraction normalized by its initially uniform value C_0. All dimensions are normalized by L. The square root of the characteristic ratio of the EM body force to the viscous forces is the Hartmann number $Ha = BL(\sigma/\mu)^{1/2}$, where μ is the viscosity of the melt. The characteristic ratio of convective to conductive heat transfer is the thermal Péclet number $Pe_t = \rho_0^2 g\beta_c C_0 c_p L/k\sigma B^2$, where c_p and k are the specific heat and thermal conductivity of the melt, respectively. The characteristic ratio of convective to diffusive species transfer is the mass Péclet number $Pe_m = \rho_0 g\beta_c C_0 L/\sigma B^2 D$.

For a sufficiently strong magnetic field $Pe_t \ll 1$, convective heat transfer is negligible, and the crystal-melt interface is planar, as shown in Fig. 1. In general, $U_g \leq U_c$, so that the heat released by the cooling melt is negligible compared to the conductive heat transfer.[16] Therefore, the heat flux through the melt is uniform and constant, and the deviation of the melt's temperature from T_0, normalized by Lq/k, where q is the constant uniform heat flux into the right end of the container, is

$$T = x - \omega t \tag{5}$$

As the magnetic field strength is decreased and the ratio of convective heat transfer to conductive heat transfer increased, convective heat transfer caused the shape of the crystal-melt interface to deviate from planar. This effect will be investigated in a future study.

In an asymptotic solution for $Ha \gg 1$, the melt is divided into an inviscid core, Hartmann layers with an $\mathcal{O}(Ha^{-1})$ thickness adjacent to the crystal–melt interface at $\xi = -1$, and parallel layers with an $\mathcal{O}(Ha^{-1/2})$ thickness adjacent to the container walls at $y = \pm 1$. The Hartmann layers have a simple, local, exponential structure, which matches a transverse core or parallel-layer velocities at $\xi = \pm 1$, which satisfies the no-slip conditions at the solid–liquid interfaces, and which indicates that u in the core or parallel layer is $\mathcal{O}(Ha^{-1})$ at $x = \omega t$ and $x = a$. Analysis of the parallel layers reveals that their thicknesses are actually $\mathcal{O}\{[(a - \omega t)/Ha]^{1/2}\}$. Because a can be as large as 35 (Ref. 6), the parallel layer is not actually thin as assumed in the formal asymptotic expansion for $Ha \gg 1$. Although a formal asymptotic analysis for $Ha \gg 1$ is not appropriate, the numerical solution of the inertia-less Navier–Stokes equation with all viscous terms is not necessary. The Hartmann layers represent an extremely small fraction of the melt length and have a simple exponential structure. There is no need to duplicate numerically this simple exponential structure. Therefore, we use a hybrid solution that does not assume that the parallel-layer thickness is small. We discard the viscous terms $Ha^{-2}\partial^2 \boldsymbol{v}/\partial x^2$ in the Navier–Stokes equation, we relax the no-slip conditions at both $\xi = \pm 1$ because they are satisfied by the Hartmann layers that are not part of the composite solution, and we apply the boundary conditions

$$u = 0 \qquad \text{at} \qquad \xi = \pm 1 \tag{6}$$

We apply the no-slip and no-penetration conditions at $y = \pm 1$.

For our two-dimensional flow the stream function is governed by

$$Ha^{-2}\frac{\partial^4 \psi}{\partial y^4} - \frac{4}{(a - \omega t)^2}\frac{\partial^2 \psi}{\partial \xi^2} = \frac{2}{a - \omega t}\left(\gamma \frac{\partial T}{\partial \xi} + \frac{\partial C}{\partial \xi}\right) \tag{7a}$$

$$u = \frac{\partial \psi}{\partial y} \tag{7b}$$

$$v = -\frac{2}{a - \omega t}\frac{\partial \psi}{\partial \xi} \tag{7c}$$

where T is given by Eq. (5). Here $\xi = [2x - (a + \omega t)]/(a - \omega t)$ is our rescaled axial coordinate so that $-1 \leq \xi \leq 1$ for all time.

For the species transport the boundary condition at the crystal-melt interface is

$$\frac{\partial C}{\partial \xi} = -\frac{(a - \omega t)}{2} Pe_g(1 - k_s)C \qquad \text{at} \qquad \xi = -1 \tag{8}$$

where $Pe_g = U_g L/D = \omega Pe_m$ is the growth Péclet number. Along each of the other surfaces, there cannot be diffusion of species into the impermeable container, so that $\nabla C \cdot \hat{\boldsymbol{n}} = 0$, where $\hat{\boldsymbol{n}}$ is the unit normal vector.

In a previous study[8] we used an asymptotic method to treat Eq. (4a) for $\gamma = 1$ and without the $\partial C/\partial \xi$ term, Eq. (4d) with $Pe_t \ll 1$, and Eq. (4e) for the entire period of time needed grow the entire crystal. This study only considered nearly pure crystals with very small dopant concentrations so that there was only thermally driven buoyant convection, and we used the characteristic velocity $U_c = \rho_0 g\beta_T(\Delta T)_0/\sigma B^2$ for magnetically damped thermally driven buoyant convection[17] instead of Eq. (1). Here, $\boldsymbol{v}$ and $\boldsymbol{T}$ were independent of C and were known at each time step, so that Eq. (4e) was a linear equation for C with known spatially variable coefficients given by $\boldsymbol{v}$. We solved Eq. (4e) using a Chebyshev spectral collocation method with a second-order-implicit time-integration scheme for the species transport of a dopant in the molten semiconductor.

We use a Chebyshev spectral collocation method for the spatial derivatives in Eq. (4a) for the melt motion and in Eq. (4e) for the species transport with Gauss–Lobatto collocation points in ξ and y. For the time derivative in Eq. (4e), we use an implicit second-order time integration to integrate from $t = 0$ to a t that is slightly less than a/ω. We use a large enough number of time steps such that the results do not change by increasing the number of time steps and a large enough number of collocation points in each direction for both the stream function and concentration at each time step so that the velocity and concentration gradients are resolved.

At the beginning of crystal growth, the concentration of silicon, normalized with the initial uniform concentration, is $C(\xi, y, t = 0) = 1$. Thus the amount of silicon initially in the melt is obtained by integrating across the ampoule's volume giving a total dimensionless silicon concentration equal to $2a$. We verify that the sum of the total silicon in the melt and in the crystal is equal to $2a$ at each time step.

Assuming that there is no diffusion of dopant in the solid crystal, $C_s(x, y)$, normalized by the initial uniform concentration in the melt, is given by

$$C_s(x, y) = k_s C(\xi = -1, y, t = x/\omega) \tag{9}$$

where the segregation or partition coefficient for silicon in germanium is $k_s = 4.2$ for silicon in a germanium melt. The segregation coefficient is the ratio of the slope of the liquidus curve to the slope of the solidus curve on the binary phase diagram for germanium-silicon.

In the classical well-mixed limit the rejected germanium is instantly uniformly mixed over the volume of the melt at each time. In this limit the crystal composition is given by

$$C_{s,\text{avg}}(x) = k_s(1 - x/a)^{-(1 - k_s)} \tag{10}$$

In the classical diffusion-controlled limit the crystal concentration is uniform at the melt's initial uniform composition $C = 1$ except for the first-grown and last-grown parts of the crystal. In the initial and final transients corresponding to the first-grown and last-grown parts of the crystal, respectively, the crystal compositions are given by exponential curves, which are functions of k_s and Pe_g (Ref. 18).

Results

For a typical Bridgman process used to grow germanium-silicon crystals, the growth rate is $U_g = 0.1$ μm/s. For this example with $B = 2$ T, $C_0 = 0.04$ and $a = 1$, $U_c = 0.000337$ m/s, the dimensionless parameters are $\omega = 0.000297$, $Ha = 793.33$, $Pe_m = 126.42$, and the dimensionless time to grow the crystal is 3371.2.

Initially, the concentration in the melt is uniform so that the melt motion is entirely caused by thermally driven buoyant convection, as shown in Fig. 2, where the maximum value of the streamfunction is $\psi_{\max} = 0.0129$. The hotter fluid near $\xi = +1$ flows vertically upward and flows to the left for $y > 0$. When the fluid reaches the colder end of the container near the crystal-melt interface, the fluid flows vertically downward, and either solidifies or turns and flows to the right for $y < 0$. Because the temperature gradient is uniform, the streamlines are symmetric about $\xi = 0$.

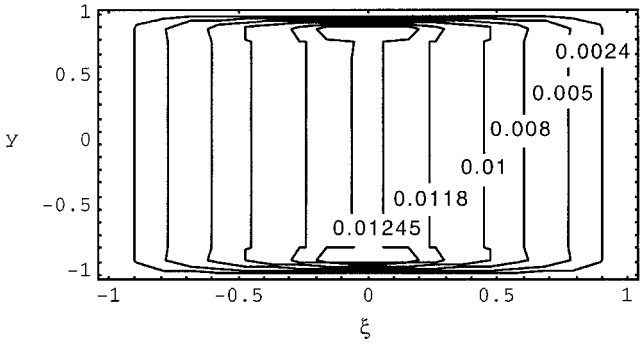

Fig. 2 Stream function in the melt at the beginning of growth $\psi(\xi, y, t = 0)$.

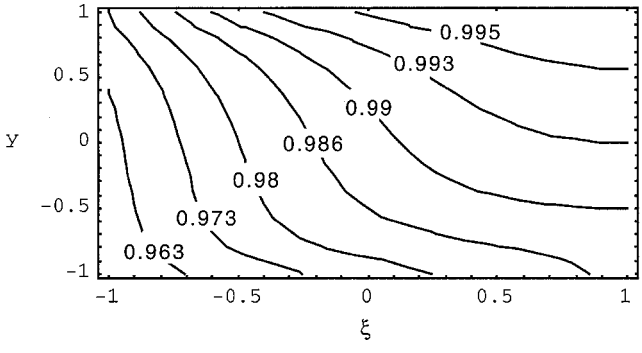

a) $C(\xi, y, 33.71)$

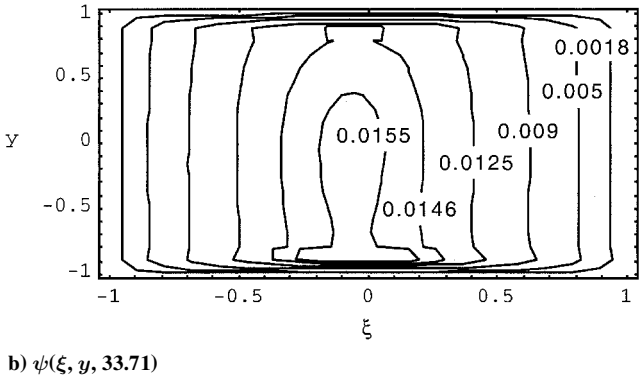

b) $\psi(\xi, y, 33.71)$

Fig. 3 Contours of the concentration and stream function in the melt at $t = 33.71$.

Once crystal growth begins, the germanium absorbs silicon as it solidifies, which then creates a silicon-depleted region adjacent to the crystal–melt interface. Just after growth begins, this concentration gradient is primarily axial and drives an axial diffusion of silicon toward the crystal–melt interface. When 1% of the crystal has grown at $t = 33.71$, the maximum value of the stream function has increased to $\psi_{max} = 0.0164$, and the minimum and maximum values of the concentration are 0.951 and 0.996, respectively, as shown in Figs. 3a and 3b. The crystal has already absorbed so much silicon that $C < 1$ everywhere in the melt. This compositionally driven buoyant convection caused by the rejection of the heavier germanium adjacent to the crystal–melt interface sinks so that it flows in the same direction as the thermally driven buoyant convection thus increasing the flow rate. This is reflected in the larger value of ψ_{max} compared with the thermally driven buoyant convection alone at $t = 0$. Even at this early stage, the large velocity adjacent to the bottom wall has carried the silicon-depleted melt to the right end of the container. The concentration gradient is larger near the crystal–melt interface at $\xi = -1$ so that the streamlines are no longer symmetric about $\xi = 0$.

The contours of the concentration and stream function are shown in Figs. 4a and 4b, respectively, for $t = 2022.71$ when 60% of the

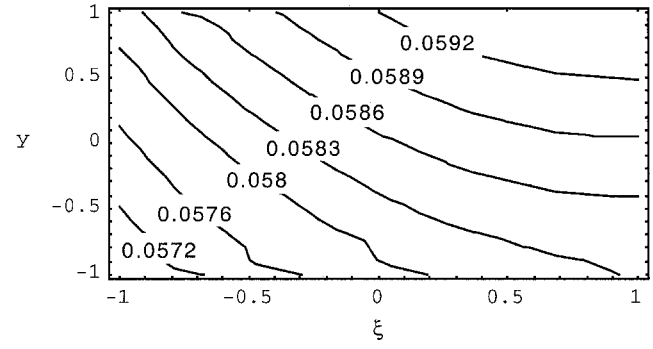

a) $C(\xi, y, 2022.7)$

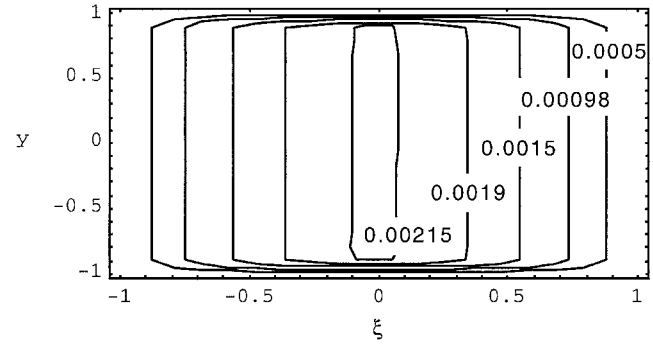

b) $\psi(\xi, y, 2022.7)$

Fig. 4 Contours of the concentration and stream function in the melt at $t = 2022.7$.

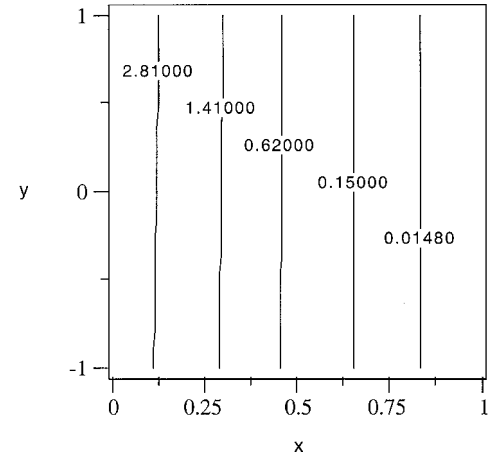

Fig. 5 Contours of the concentration in the crystal $C_s(x, y)$.

crystal has grown. At this stage the maximum value of the stream function is 0.00217, and the minimum and maximum values of the concentration are 0.0569 and 0.0595, respectively. The average concentration in the melt has decreased as a result of the absorption of silicon at the crystal–melt interface. This absorption has decreased the concentration gradient so that the magnitude of the buoyant convection has decreased as reflected in the decrease in ψ_{max}.

The contours of the concentration in the crystal are presented in Fig. 5. Because the difference between the maximum and minimum concentrations in the melt at all times is relatively small, the lateral variation of the concentration is small. The concentration along $y = -1$ in the crystal is always the lowest because there is a stagnation point in the flow at $y = -1$ and very near $\xi = -1$, so that the nearly stagnant fluid near $y = -1$ and $\xi = -1$ always loses a larger amount of silicon before solidifying. The axial variation of the laterally averaged concentration in the crystal is presented in Fig. 6. The axial decrease of the laterally averaged C_s, which is evident in Fig. 5, is reflected in Fig. 6. The silicon that is absorbed from the melt at the crystal–melt interface has the effect of decreasing the

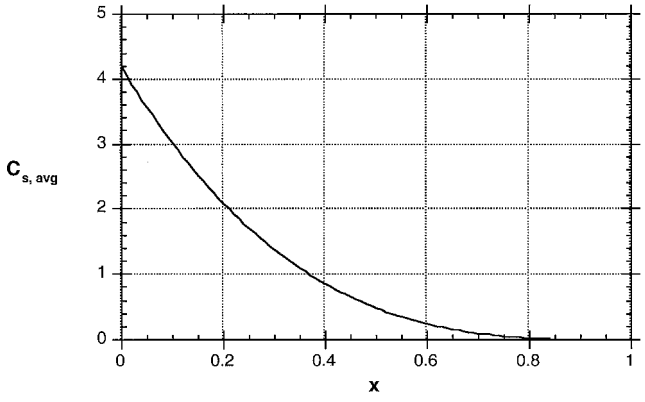

Fig. 6 Axial variation of the laterally averaged crystal concentration $C_{s,avg}(x)$.

average melt concentration, which then decreases the crystal concentration after the silicon-depleted melt is convected back towards the crystal–melt interface. Near the end of growth, the crystal has absorbed virtually all of the silicon, so that the right end of the crystal has $C_s = 0$. The laterally averaged concentration in Fig. 6 very nearly coincides with the classical well-mixed values even though the concentration in the melt is very nonuniform at all times.

Conclusions

During the horizontal Bridgman process with a steady magnetic field, the large horizontal velocity quickly convects the silicon-depleted melt from a region adjacent to the crystal–melt interface to the right end of the container so that the concentration difference in the melt is small. The crystal solidifies with little lateral segregation. Because of the large value of the segregation coefficient, the axial variation of the concentration in the crystal is large but very nearly resembles the well-mixed limit.

Acknowledgments

This research was supported by NASA under Grant NAG8-1817. The calculations were performed on IBM SP at the North Carolina Supercomputing Center in Research Triangle Park, North Carolina.

References

[1]Chedzey, H. A., and Hurle, D. T. J., "Avoidance of Growth-Striae in Semiconductor and Metal Crystals Grown by Zone-Melting Techniques," *Nature*, Vol. 210, 1966, pp. 933–934.

[2]Utech, H. P., and Flemings, M. C., "Elimination of Solute Banding in Indium Antimonide Crystals by Growth in a Magnetic Field," *Journal of Applied Physics*, Vol. 7, 1966, pp. 2021–2024.

[3]Kim, D. H., Adornato, P. M., and Brown, R. A., "Effect of Vertical Magnetic Field on Convection and Segregation in Vertical Bridgman Crystal Growth," *Journal of Crystal Growth*, Vol. 89, No. 2/3, 1988, pp. 339–356.

[4]Watring, D. A., and Lehoczky, S. L., "Magneto-Hydrodynamic Damping of Convection During Vertical Bridgman-Stockbarger Growth of HgCdTe," *Journal of Crystal Growth*, Vol. 167, Nos. 3/4, 1996, pp. 478–487.

[5]Ramachandran, N., and Watring, D. A., "Convection Damping by an Axial Magnetic Field During Growth of HgCdTe by Vertical Bridgman Method—Thermal Effects," AIAA Paper 97-0450, Jan. 1997.

[6]Watring, D. A., "Effects of Static Axial Magnetic Fields on Directional Solidification of HgCdTe," Ph.D. Dissertation, Dept. of Mechanical Engineering and Materials Sciences, Massachusetts Inst. of Technology, Cambridge, MA, 1997.

[7]Hart, J. E., "On Sideways Diffusive Instability," *Journal of Fluid Mechanics*, Vol. 49, 1971, pp. 279–288.

[8]Hirtz, J. M., and Ma, N., "Dopant Transport During Semiconductor Crystal Growth. Axial Versus Transverse Magnetic Fields," *Journal of Crystal Growth*, Vol. 210, No. 4, 2000, pp. 554–572.

[9]Ma, N., "Solutal Convection During Melt Growth of Alloyed Semiconductor Crystals in a Steady Magnetic Field," AIAA Paper 2002-1113, Jan. 2002.

[10]Hurle, D. T. J., and Series, R. W., "Use of a Magnetic Field in Melt Growth," *Handbook of Crystal Growth*, Vol. 2A, Elsevier, Amsterdam, 1994, pp. 261–285.

[11]Garandet, J. P., and Alboussière, T., "Bridgman Growth: Modelling and Experiments," *Progress in Crystal Growth and Characterization of Materials*, edited by K. W. Benz, Vol. 38, Elsevier, Amsterdam, 1999, pp. 73–132.

[12]Walker, J. S., "Models of Melt Motion, Heat Transfer and Mass Transport During Crystal Growth with Strong Magnetic Fields," *Progress in Crystal Growth and Characterization of Materials*, edited by K. W. Benz, Vol. 38, Elsevier, Amsterdam, 1999, pp. 195–213.

[13]Walker, J. S., and Ma, N., "Convective Mass Transport During Bulk Growth of Semiconductor Crystals with Steady Magnetic Fields," *Annual Review of Heat Transfer*, edited by C.-L. Tien, V. Prasad, and F. Incropera, Vol. 12, Begell House, New York, 2002, pp. 223–263.

[14]Alboussière, T., Neubrand, A. C., Garandet, J. P., and Moreau, R., "Segregation During Horizontal Bridgman Growth Under an Axial Magnetic Field," *Journal of Crystal Growth*, Vol. 181, Nos. 1/2, 1997, pp. 133–144.

[15]Ma, N., and Walker, J. S., "Inertia and Thermal Convection During Crystal Growth with a Magnetic Field," *Journal of Thermophysics and Heat Transfer*, Vol. 15, No. 1, 2001, pp. 50–54.

[16]Ma, N., and Walker, J. S., "Dopant Transport During Semiconductor Crystal Growth with Magnetically Damped Buoyant Convection," *Journal of Crystal Growth*, Vol. 172, Nos. 1/2, 1997, pp. 124–135.

[17]Hjellming, L. N., and Walker, J. S., "Melt Motion in a Czochralski Crystal Puller with an Axial Magnetic Field: Motion Due to Buoyancy and Thermocapillarity," *Journal of Fluid Mechanics*, Vol. 182, 1987, pp. 335–368.

[18]Flemings, M. C., *Solidification Processing*, McGraw–Hill, New York, 1974, pp. 41–43.